Published in final edited form as:
Chem Sci. 2012 ; 3(1): . doi:10.1039/C1SC00499A.

Lipid-Coated Nanoscale Coordination Polymers for Targeted Delivery of Antifolates to Cancer Cells

Rachel C. Huxford[+], **Kathryn E. deKrafft**[+], **William S. Boyle**, **Demin Liu**, and **Wenbin Lin**
Department of Chemistry, CB#3290, University of North Carolina, Chapel Hill, NC 27599, USA
Fax: 1-919-962-2388; Tel: 1-919-962-6320

Wenbin Lin: wlin@unc.edu

Abstract

Nanoscale coordination polymers (NCPs) have been demonstrated as an interesting platform for drug delivery, as they possess many advantages over small-molecule chemotherapeutics, such as high payloads, lower systemic toxicity, tunability, and enhanced tumor uptake. Existing formulations for the delivery of methotrexate (MTX), an antifolate cancer drug, have very low drug loadings. Herein, we report the incorporation of MTX as a building block in an NCP formulation with exceptionally high drug loadings (up to 79.1 wt%) and the selective delivery of the NCP to cancer cells. Encapsulation of the NCP in a functionalized lipid bilayer allows for targeted delivery and controlled release to cancer cells. A phosphor can be doped into the NCPs for monitoring particle uptake by optical imaging. The lipid-coated and anisamide-targeted NCPs have superior *in vitro* efficacy against acute lymphoblastic leukemia cells when compared to free drug.

Introduction

Coordination polymers, also known as metal-organic frameworks (MOFs), have recently emerged as an interesting class of hybrid materials comprised of organic bridging ligands coordinatively bound to metal-connecting points.[1–2] The highly tunable nature of coordination polymers has allowed the design of numerous promising materials for a number of applications, including catalysis,[3–8] nonlinear optics,[9] light harvesting,[10] selective gas adsorption,[11–12] chemical sensing,[13–16] and gas storage.[17–22] When these materials are scaled down to the nano-regime to afford nanoscale coordination polymers (NCPs), they can be exploited for a number of biomedical applications.[23–26] For example, we and others have demonstrated the potential utility of NCPs in magnetic resonance imaging,[27–32] computed tomography,[33] optical imaging,[34–35] and biosensing.[36] Whereas Horcajada and coworkers demonstrated the delivery of chemotherapeutics in the pores of the MIL family of NCPs,[37] our group successfully delivered cisplatin prodrugs by either direct incorporation of the prodrug into an NCP or by postsynthetic covalent attachment of a prodrug to a pre-synthesized NCP.[38–39] In this work, we are utilizing a different direct

Correspondence to: Wenbin Lin, wlin@unc.edu.

[+]These authors contributed equally to this work.

[†]Electronic Supplementary Information (ESI) available: General experimental; SEM images of **1, 2, 3a, 4a**, $Ru(bpy)_3^{2+}$-doped **3a**, and $Ru(bpy)_3^{2+}$-doped **4a**; TEM images of liposomes, **1, 2, 3a**, and **3b**; PXRD of **1**; DLS of liposomes, **1, 2**, and **3a**; UV-Vis spectra of MTX, **3a**, and $Ru(bpy)_3^{2+}$-doped **3a**; release profiles of **2** and coated **2** in PBS and SBF; preparation of SBF; confocal images of $Ru(bpy)_3^{2+}$-doped **3b** coated in 10 mol% DOPE-FITC liposomes; synthesis of DOPE-FITC; *in vitro* cytotoxicity procedure and curves for **1** and **2**; *in vitro* cytotoxicity curves for **3a**–**c**; *in vitro* viability assays for **4a–c** and Gd^{3+}; and confocal images of Jurkat cells incubated with **4a–c**. See DOI: 10.1039/b000000x/

incorporation strategy to deliver organic antifolate chemotherapeutics possessing functional groups that can bridge metal-connecting points in NCP formulations.[40–41]

Methotrexate (MTX) is a small molecule chemotherapeutic agent that works by inhibiting dehydrofolate reductase, thereby preventing DNA synthesis. While MTX is toxic to many cancer cells and is the first-line treatment for acute lymphoblastic leukemia (ALL), its efficacy is compromised by an array of drawbacks, including poor pharmacokinetics, low tolerated doses, and resistance.[42] Large doses of MTX are required as a result of its non-specific distribution and rapid renal clearance, which can lead to systemic toxicity. Prolonged MTX treatment of ALL patients can result in numerous side effects such as mucositis, hematological toxicity, and secondary cancer. Drug delivery with nanoparticulate carriers can overcome many of the drawbacks of conventional chemotherapy, as nanoparticles can carry a large payload and significantly improve tumor uptake by taking advantage of the enhanced permeation and retention (EPR) effect.[43] Drug encapsulation in liposomes has, for example, led to enhanced efficacy due to improved pharmacokinetics.[44] Tumor uptake of nanotherapeutics can be further improved by surface conjugation of affinity molecules that bind to certain receptors overexpressed by cancer cells.[43]

Although several nanoparticle systems have been examined for MTX delivery, relatively low drug loadings were achieved in these studies.[45–50] We hypothesized that MTX can be incorporated into NCPs as a bridging ligand since it contains two carboxylate groups which can coordinate to metal connecting points. Very high loadings of MTX can be achieved in such NCP formulations. Thus, we wish to report the synthesis and characterization of MTX-based NCPs, their stabilization and cancer targeting with a lipid bilayer, and *in vitro* efficacy against Jurkat ALL cells (Scheme 1). A carboxylic acid derivative of luminescent $Ru(bpy)_3^{2+}$ (bpy = 2,2'-bipyridine) was also incorporated into the NCPs to allow the monitoring of MTX uptake by cancer cells via confocal microscopy.

Experimental Section

Synthesis of Zn-MTX NCP (1)

NCPs of **1** were synthesized by a high-temperature surfactant-assisted method. Two microemulsions with W=15 were prepared by the addition of 270 μL of an aqueous solution of MTX dimethylammonium salt (0.10 M, pH=10.6) and 270 μL of an aqueous solution of $Zn(NO_3)_2{\cdot}6H_2O$ (0.11 M) to separate 10 mL aliquots of a 0.1 M CTAB/0.5 M 1-hexanol/isooctane mixture. The separate microemulsions were stirred vigorously for 10 min at room temperature, then the two microemulsions were combined, and the resultant 20 mL microemulsion with W=15 was transferred to a sealed microwave vessel. The reaction was rapidly heated to 120 °C, and held at this temperature for 10 min with stirring. After cooling, the nanoparticles were isolated by centrifugation at 13,000 rpm for 10 min. After the removal of the supernatant, the particles were washed twice, using 10 mL of ethanol each time. For each wash, the particles were redispersed by sonication and then recovered by centrifugation at 13,000 rpm for 10 min. Yield: 11.8 mg (84.2%).

Synthesis of Zr-MTX NCP (2)

$ZrCl_4$ (6.99 mg, 0.03 mmol) was dissolved in 6 mL N,N-dimethylformamide (DMF), followed by 13.67 mg (0.03 mmol) methotrexate. The clear yellow solution was placed in a sealed microwave vessel and heated at 60 °C for 5 minutes (300 W, 200 psi) without stirring. The product was isolated from the resulting yellow dispersion by centrifugation at 13,000 rpm for 15 min, washed by sonication and centrifugation, with H_2O then EtOH, and dispersed in EtOH. Yield: 8.88 mg (54.4%).

Synthesis of Gd-MTX NCP (3a)

Both $Gd(NO_3)_3{\cdot}6H_2O$ (13.54 mg, 0.0300 mmol) and MTX (13.63 mg, 0.0300 mmol) were dissolved in 6 mL DMF and the solution was heated in a sealed microwave vessel at 80 °C for 5 min without stirring. The product was isolated from the resulting yellow dispersion by centrifugation at 13,000 rpm for 15 min, washed by sonication and centrifugation, with DMF then EtOH, and dispersed in EtOH. Yield: 15.6 mg (85%).

Synthesis of Gd-folate NCP (4a)

22.5 mg (0.0498 mmol) $Gd(NO_3)_3{\cdot}6H_2O$ was dissolved in 3 mL DMF, and 22.2 mg (0.0503 mmol) folic acid was dissolved in 7 mL DMF by heating. The procedure was similar to that of **3a**. Yield: 7.5 mg (25.2%).

Synthesis of [Ru(5,5'-CO_2-bpy)(bpy)$_2$]-doped analogs of 3a–c and 4a–c

10 mol% [Ru(5,5'-CO_2-bpy)(bpy)$_2$]-doped **3a** was synthesized by the same procedure as **3a**, but with the addition of 2.02 mg (0.00308 mmol, 10 mol%) [Ru(5,5'-CO_2Hbpy)(bpy)$_2$] $(PF_6)_2$ to the DMF solution. Particles were isolated in a yield of 20.9 mg (72%). 10 mol% [Ru(5,5'-CO_2-bpy)(bpy)$_2$]-doped **4a** was synthesized by the same procedure as **4a**, but with the addition of 3.3 mg (0.0050 mmol, 10 mol%) Ru(bpy)$_2$(bby-CO_2H) to the DMF solution. Particles were isolated in a yield of 9.45 mg (29%). Synthesis of lipid-coated versions of doped **3a** and **4a** were carried out by the same methods for **3b, 3c, 4b**, and **4c**.

Synthesis of Lipid-Coated NCPs

a). Synthesis of DSTAP/DOPE-coated 3a—Particle dispersions of **3a** and 1:1 (by mol) DSTAP/DOPE liposomes in 1 mM aq. KCl were heated to 70 °C and mixed together. The dispersion was vortexed and was allowed to sit at room temperature for 30 minutes. Empty liposomes were removed by centrifugation at 6,000 rpm for 10 minutes, and the resulting particles of **3b** were redispersed in 1 mM aq. KCl by sonication.

b). Synthesis of DSTAP/DOPE-AA-coated 3a—These lipid-coated particles were produced by the same technique as **3b**, but using 1:1 (by mol) DSTAP/DOPE liposomes, incorporating 10 mol% DOPE-AA.

Cytotoxicity assay of 3a, 3b, and 3c against Jurkat cells

Confluent Jurkat cells were counted from the culture flask by hemocytometer. Cells were plated in 6-well plates at a cell density of 5×10^4 cells/well in 1.5 mL RPMI-1640 complete growth medium. The cells were incubated at 37 °C and 5% CO_2 overnight. MTX and particle dispersions of **3a, 3b**, and **3c** (16 μM) in RPMI-1640 media and additional media were added to wells, resulting in MTX concentrations (μM) of 0, 0.25, 0.5, 1, 2, and 4. Cells were incubated (37 °C, 5% CO_2) with free MTX or particle for 48 h or for 72 h. Viability was determined by the trypan blue exclusion assay.

Viability control assays with Jurkat cells

This assay was conducted to show that MTX is the only contributor to cytotoxicity and that Gd^{3+} has no bearing on the cytotoxicity. $Gd(NO_3)_3$, **4a, 4b**, and **4c** were tested against Jurkat acute lymphoblastic leukemia cells. Confluent Jurkat cells were counted from the culture flask by hemocytometer. Cells were plated in 6-well plates at a cell density of 5×10^4 cells/well in 1.5 mL RPMI-1640 complete growth medium. The cells were incubated at 37 °C and 5% CO_2 overnight. Free Gd^{3+} and particle dispersions (200 μM) in RPMI-1640 media and additional media were added to wells, resulting in folate concentrations (μM) of

0, 0.5, 1, 2.5, 5, and 10. Cells were incubated (37 °C, 5% CO_2) with free Gd^{3+} or particles for 48 h. Viability was determined by the trypan blue exclusion assay.

Confocal microscopy of [Ru(5,5'-CO_2-bpy)(bpy)$_2$]-doped analogs of 3a–c and 4a–c

Wells in 6-well plates were seeded with 500,000 cells and 2 mL total of RPMI-1640 media (10% FBS, 2% penicillin-streptomycin). The plates were incubated for 24 h at 37 °C and 5% CO_2. Particle dispersions were prepared in RPMI-1640 medium, and aliquots of particle dispersions/additional media were added to the wells, resulting in a concentration of 0.04 mg/well for each particle. The cells were incubated with particles for 1 h, and cell suspensions were centrifuged. Cell pellets were re-suspended in PBS, 15 μL Annexin V FITC conjugate was added, and the cells were allowed to sit at room temperature for 10 min. The cells were centrifuged and redispersed in 20μL of media. The entire cell suspension was placed on glass coverslips, adhered on glass slides with antifade mounting medium, and imaged at the UNCCH Microscope and Imaging Facility.

Results and Discussion

Synthesis and Characterization of MTX-Containing NCPs

Three new NCPs were synthesized using MTX as the bridging ligand and either Zn^{2+}, Zr^{4+}, or Gd^{3+} ions as the metal-connecting points. The properties of the NCPs, especially stability, can be tuned by the choice of metal ion. Zn^{2+} was originally chosen as the metal linker for a MTX-containing NCP due to its biocompatibility. Zn-MTX (**1**) was synthesized in 84% yield by first preparing a microemulsion of 0.1 M CTAB (CTAB = cetyltrimethylammonium bromide) and 0.5 M 1-hexanol in isooctane with a water-to-surfactant ratio (W) of 15, containing $[CH_3NH_3]_2$(MTX) and $Zn(NO_3)_2$. Surfactant-assisted synthesis was carried out by microwave heating of the microemulsion in a sealed vessel at 120 ° C for 10 min, with stirring. The particles were isolated by centrifugation and washed with ethanol. Both scanning electron microscopy (SEM) and transmission electron microscopy (TEM) showed that particles of **1** are spherical with a diameter between 40 and 100 nm (Fig 1a). Dynamic light scattering (DLS) in ethanol gives a number average size of 161 nm, slightly larger than the size observed by microscopy due to slight aggregation in this medium. These particles were shown by thermogravimetric analysis (TGA) (Fig. 2a) to contain 79.1 wt% MTX based on the organic weight loss. Powder X-ray diffraction (PXRD) reveals the amorphous structure of these particles by the lack of diffraction peaks (Fig. S3). Attempts were made to coat **1** with a biocompatible shell (either silica or a lipid bilayer), but the particles were not stable under coating conditions. Coating **1** with a layer of silica by hydrolysis and condensation of tetraethylorthosilicate (TEOS) was unsuccessful because the ammonium hydroxide catalyst causes severe erosion of the particles. Lipid-coating of **1** also failed due to particle agglomeration in aqueous media. Additionally, the zeta potential of the particles is close to neutral (−1.9 mV), precluding efficient electrostatic interactions with positively-charged liposomes.

We hypothesized that more robust NCPs could be synthesized using Zr^{4+} in place of Zn^{2+} metal-connecting points, due to the strength of the Zr-carboxylate bond.[51] Zr-MTX (**2**) was synthesized in 54% yield by microwave heating of a solution of MTX and $ZrCl_4$ in N,N-dimethylformamide (DMF) at 60 °C for 5 min in a sealed vessel. The resulting spherical particles had a diameter of 70 to 180 nm by both SEM and TEM (Fig. 1b), and 88.4 nm by DLS (Fig. 2b). Particles of **2** had a high MTX loading of 78.2% by TGA. As-synthesized **2** had a zeta potential (1 mM aq. KCl) of −27.2 mV. This negative zeta potential, along with stability in water, allows for coating of these particles with a cationic lipid bilayer to provide biocompatibility and stabilization in physiologically relevant media.[52–54] **2** was coated with different liposomal formulations, such as 4:48:48 (by mol) DOTAP/DOPE/cholesterol

(DOTAP = dioleoyl trimethylammonium propane and DOPE = dioleoyl L-α-phosphatidylethanolamine), 1:1 (by mol) DOTAP/cholesterol, DOTAP, DSTAP (DSTAP = 1,2-stearoyl-3-trimethylammonium propane), and 1:1 (by mol) DSTAP/DOPE. Different liposomal formulations were made by drying a chloroform solution of lipids to create a film that was then hydrated with 1 mM aq. KCl. The resulting liposomes were extruded through polycarbonate membranes several times to obtain unilamellar vesicles with sizes ranging from 25–160 nm, depending on the formulation. Zeta potentials ranged from 50 to 60 mV. Dispersions of liposomes and **2** were mixed together, and empty liposomes were removed by centrifugation at low speed. Coating occurs by rearrangement of the cationic liposomes onto the anionic surface of the particles, resulting in encapsulation of **2** in a lipid bilayer. Lipid coating of **2** was verified by an increase in the zeta potential from −27.2 mV to 25–50 mV. However, lipid coating failed to provide any significant stabilization over the as-synthesized particles in phosphate buffered saline (PBS) or simulated body fluid (SBF). The half-life for both coated and bare particles was approximately 2.5 h in PBS and 0.5 h in SBF at 37 °C and pH = 7.4 (Fig. S6, S7). We speculate that lipid coating failed to stabilize **2** owing to the strong driving force in forming $Zr_3(PO_4)_4$ in the presence of phosphate ions. For comparison, $Zr_3(PO_4)_4$ has a K_{sp} value of 10^{-134} while $Zn_3(PO_4)_2$ has a K_{sp} value of 10^{-34}.

Considering our inability to stabilize **1** and **2**, we rationalized that a formulation containing a metal less labile than zinc, but with a phosphate K_{sp} much greater than that of $Zr_3(PO_4)_4$, would prove easier to stabilize by lipid coating. Trivalent lanthanide ions have much greater K_{sp} values (10^{-23} for $Gd(PO_4)$ and should provide a good balance between particle stability and lipid stabilization toward lanthanide phosphate formation. Gd-MTX NCP, **3a**, was synthesized in 85% yield by microwave heating of a solution of MTX and $Gd(NO_3)_3$ in DMF at 80 ° C for 5 min in a sealed vessel. The as-synthesized particles of **3a** were spheres of 70 to 200 nm by SEM and TEM (Fig. 1c) and 77.7 nm by DLS (Fig. 2b). By TGA, these particles contain 71.6 wt% MTX (Fig. 2a). With a zeta potential (1 mM aq. KCl) of −10.0 mV, **3a** can be coated with a cationic liposome in order to further stabilize these particles.

Stabilization of Gd-MTX NCP With A Lipid Bilayer

The half-life of **3a** is only 2 h in 8 mM PBS at 37 °C, and needs to be prolonged for many biological applications (Fig. 2c). Stabilization with a lipid bilayer was pursued, due to the biocompatibility and known biological stability of this coating.[52–54] Thus, **3a** was coated with a 1:1 (by mol) DSTAP/DOPE liposomal formulation. These liposomes were made as previously discussed and had an average size of 94.3 nm and a zeta potential of 59.5 mV by DLS. The liposomes were mixed with a particle dispersion of **3a** in 1 mM aq. KCl at a 10:1 particle:lipid weight ratio to obtain **3a** encapsulated in a lipid bilayer (**3b**). Complete coverage is indicated by an increase in the zeta potential to 32.6 mV, and a size similar to the as-synthesized particles. Complete coverage of individual particles with a lipid bilayer was confirmed by TEM (Fig. 1f). **3b**, when stained with 5% aq. uranyl acetate, exhibited dark rings around each particle due to strong binding of uranyl ions with the phosphates of DOPE in the lipid bilayer.[55] The lipid bilayer stabilized the particles against dissolution, as evidenced by a release profile in 8 mM PBS (37 °C, pH = 7.4). MTX release was monitored by UV-Vis spectroscopy as the particles were dialyzed. The half-life of **3b** was 23 h, compared to $t_{1/2}$ = 2 h for **3a**, with 100% release at 192 h (Fig. 2c). It is worth noting that lipid-coated NCPs are individual, lipid-stabilized, solid particles and are different from conventional liposomes.[56]

In order to improve delivery of nanoparticles *in vitro*, particles can be modified with affinity molecules to target receptors which are overexpressed on the surface of tumor cells. For example, sigma receptors are overexpressed on a number of different human cancer cell

lines, including lung, colorectal, breast, and others.[57] These sigma receptors can be targeted by small benzamides, such as anisamide (AA).[58–60] For this work, we were able to conjugate AA to the primary amine of DOPE and integrate approximately 10 mol% of this lipid into the liposomal formulation before lipid coating of **3a**, resulting in AA-functionalized particles (**3c**). The particle size of **3c** is similar to that of the as-synthesized particles, and the zeta potentials are positive, indicating coverage by the cationic liposome.

Synthesis and Characterization of Gd-Folate NCP Control Vehicles

As a control, a non-cytotoxic analog of **3a** was synthesized by substituting folic acid, a naturally-occurring nutrient, for MTX to give a Gd-folate NCP (**4a**). Folic acid has a structure similar to MTX, with two carboxylic acid groups which can coordinate to metal ions. These particles were synthesized in DMF with microwave heating in a similar fashion to **3a**. The resulting particles were 200–300 nm by SEM, and 262 nm by DLS. These particles have a zeta potential of −11.8 mV (1 mM aq. KCl), and can be coated with 1:1 (by mol) DSTAP/DOPE liposomes (**4b**) and functionalized with AA (**4c**) by the methods described for **3a**. Control vehicles **4a–c** do not contain any anticancer agent and were utilized in cytotoxicity and confocal microscopy experiments as analogs of **3a–c**.

Enhanced *in vitro* Efficacy of Lipid-Coated Gd-MTX NCPs

3a, 3b, and **3c** all showed enhanced efficacy compared to free MTX *in vitro* against Jurkat human ALL cells. Jurkat cells are known to overexpress sigma receptors,[61] and can therefore be subjected to AA-targeting. Cells were incubated with MTX or NCPs for 72 h, and then viability was determined by the trypan blue exclusion assay. **3a** was slightly less cytotoxic than free MTX (IC_{50} = 34.7±2.5 nM), with an IC_{50} of 54.7±2.3 nM. Improved efficacy of **3a** over free MTX is not expected due to the rapid degradation of these particles in biological media. The lipid coating on **3b** significantly improved efficacy with an IC_{50} value of 28.3±0.6 nM; this enhancement is contributed to the affinity of cationic lipid bilayers for cell membranes. AA targeting proved successful, with **3c** having a slightly lower, statistically significant, IC_{50} (23.7±1.5 nM) than the lipid-coated formulation (Fig. 2d). Free Gd^{3+} salt and **4a–c** were also tested (Fig. S16), and did not exhibit any cytotoxic effect in the same concentration range, proving that MTX, not Gd^{3+}, is responsible for cytotoxicity of **3a**–**c**. **1** and **2** were also tested against human cancer cell lines (Fig. S13, S14), and no enhancement in efficacy over free MTX was observed, presumably due to their rapid degradation in biological media to release free MTX.

1. Optical Imaging of Gd-MTX NCPs With Jurkat Human ALL Cells

3a and **4a** were doped with approximately 10 mol% of a carboxylic acid derivative of the phosphor $Ru(bpy)_3^{2+}$ so that this platform can be used for optical imaging. Additionally, this doping strategy allows for further verification of successful lipid coating when the lipid is functionalized with FITC (fluoroscein isothiocyanate) (Fig. S9). The doped particles were synthesized in DMF by the same method as **3a** and **4a** but with the addition of 10 mol% of the $Ru(bpy)_3^{2+}$ derivative. The doped particles had similar sizes, ligand loadings, and zeta potentials compared to their undoped counterparts, allowing phosphorescent versions of **3b, 3c, 4b**, and **4c** to be made from doped **3a** and **4a**. Laser scanning confocal fluorescence microscopy was performed on Jurkat cells incubated with NCPs to assess the imaging and targeting efficiency of the NCPs. The cells were also stained with Annexin V FITC conjugate to assay for early apoptosis. As displayed in Fig. 3, co-localized fluorescence signal is observed in the cells from the $Ru(bpy)_3^{2+}$-doped particles (red) and the apoptosis stain (green) for **3b**. Significantly stronger red and green fluorescence signals are seen for **3c**, due to increased cell uptake of the targeted particles, and hence increased cytotoxicity. No red or green fluorescence was observed for **3a**, as these particles disintegrate quickly,

and do not have a mechanism to permeate the cell membrane during the 1 h incubation time for the experiment. Fluorescence from $Ru(bpy)_3^{2+}$ was observed for the cells incubated with **4b** and **4c**, similar to **3b** and **3c**. However, as expected, no apoptosis (green fluorescence) was observed for **4a–c** (Fig. S18).

Conclusions

We have successfully formulated novel NCPs containing up to 79.1 wt% methotrexate. Gd-MTX NCPs were stabilized by a DSTAP/DOPE lipid bilayer. A DOPE-AA conjugate was incorporated into the lipid bilayer and used to target sigma receptors overexpressed on leukemia cancer cells. The NCPs were doped with 10 mol% of a carboxylated $Ru(bpy)_3^{2+}$ derivative, which serves as an optical imaging agent, as evidenced by confocal microscopy of Jurkat human acute lymphoblastic leukemia cells. Finally, lipid-coated and targeted NCPs were shown to have superior efficacy compared to the as-synthesized particles or free drug in *in vitro* cytotoxicity assays with Jurkat cells. We believe that this NCP formulation strategy is general and can be applied to deliver many other organic anticancer drugs.

Supplementary Material

Refer to Web version on PubMed Central for supplementary material.

Acknowledgments

We acknowledge financial support from NIH (U01-CA1511455). We thank Ms. Stephanie Kramer for experimental help.

Notes and references

1. Robson R. J. Am. Chem. Soc., Dalton Trans. 2000:3735–3744.
2. Yaghi OM, O'Keeffe M, Ockwig NW, Chae HK, Eddaoudi M, Kim J. Nature. 2003; 423:705–714. [PubMed: 12802325]
3. Kesanli B, Lin WB. Coord. Chem. Rev. 2003; 246:305–326.
4. Lee J, Farha OK, Roberts J, Scheidt KA, Nguyen ST, Hupp JT. Chem. Soc. Rev. 2009; 38:1450–1459. [PubMed: 19384447]
5. Ma L, Abney C, Lin W. Chem. Soc. Rev. 2009; 38:1248–1256. [PubMed: 19384436]
6. Ma L, Falkowski JM, Abney C, Lin W. Nat. Chem. 2010; 2:838–846. [PubMed: 20861899]
7. Song F, Wang C, Falkowski JM, Ma L, Lin W. J. Am. Chem. Soc. 2010; 132:15390–15398. [PubMed: 20936862]
8. Wu C-D, Hu A, Zhang L, Lin W. J. Am. Chem. Soc. 2005; 127:8940–8941. [PubMed: 15969557]
9. Evans OR, Lin W. Acc. Chem. Res. 2002; 35:511–522. [PubMed: 12118990]
10. Kent CA, Mehl BP, Ma L, Papanikolas JM, Meyer TJ, Lin W. J. Am. Chem. Soc. 2010; 132:12767–12769. [PubMed: 20735124]
11. Uemura K, Kitagawa S, Fukui K, Saito K. J. Am. Chem. Soc. 2004; 126:3817–3828. [PubMed: 15038736]
12. Uemura K, Kitagawa S, Kondo M, Fukui K, Kitaura R, Chang H-C, Mizutani T. Chem. Eur. J. 2002; 8:3586–3600. [PubMed: 12203285]
13. Chen B, Wang L, Xiao Y, Fronczek FR, Xue M, Cui Y, Qian G. Angew. Chem. Int. Ed. 2009; 48:500–503.
14. Chen BL, Xiang SC, Qian GD. Acc. Chem. Res. 2010; 43:1115–1124. [PubMed: 20450174]
15. Lan A, Li K, Wu H, Olsson DH, Emge TJ, Ki W, Hong M, Li J. Angew. Chem. Int. Ed. 2009; 48:2334–2338.
16. Xie Z, Ma L, deKrafft KE, Jin A, Lin W. J. Am. Chem. Soc. 2009; 132:922–923. [PubMed: 20041656]

17. D'Alessandro DM, Smit B, Long JR. Angew. Chem. Int. Ed. 2010; 49:6058–6082.
18. Dinca M, Long JR. Angew. Chem. Int. Ed. 2008; 47:6766–6779.
19. Furukawa H, Ko N, Go Y-B, Aratani N, Choi SB, Choi E, Yazaydin AO, Snurr RQ, O'Keeffe M, Kim J, Yaghi OM. Science. 2010; 329:424–428. [PubMed: 20595583]
20. Ma L, Mihalcik DJ, Lin W. J. Am. Chem. Soc. 2009; 131:4610–4612. [PubMed: 19290636]
21. Murray LJ, Dinca M, Long JR. Chem. Soc. Rev. 2009; 38:1294–1314. [PubMed: 19384439]
22. Rowsell JLC, Yaghi OM. Angew. Chem. Int. Ed. 2005; 44:4670–4679.
23. Della Rocca J, Lin W. Eur. J. Inorg. Chem. 2010:3725–3734.
24. Huxford RC, Della Rocca J, Lin W. Curr. Opin. Chem. Biol. 2010; 14:262–268. [PubMed: 20071210]
25. Lin W, Rieter WJ, Taylor KML. Angew. Chem. Int. Ed. 2009; 48:650–658.
26. Spokoyny AM, Kim D, Sumrein A, Mirkin CA. Chem. Soc. Rev. 2009; 38:1218–1227. [PubMed: 19384433]
27. Nishiyabu R, Hashimoto N, Cho T, Watanabe K, Yasunaga T, Endo A, Kaneko K, Niidome T, Murata M, Adachi C, Katayama Y, Hashizume M, Kimizuka N. J. Am. Chem. Soc. 2009; 131:2151–2158. [PubMed: 19166341]
28. Rieter WJ, Taylor KML, An H, Lin W, Lin W. J. Am. Chem. Soc. 2006; 128:9024–9025. [PubMed: 16834362]
29. Rowe MD, Chang CC, Thamm DH, Kraft SL, Harmon JF, Vogt AP, Sumerlin BS, Boyes SG. Langmuir. 2009; 25:9487–9499. [PubMed: 19422256]
30. Rowe MD, Thamm DH, Kraft SL, Boyes SG. Biomacromolecules. 2009; 13:983–993. [PubMed: 19290624]
31. Taylor KML, Jin A, Lin W. Angew. Chem. Int. Ed. 2008; 47:7722–7725.
32. Taylor KML, Rieter WJ, Lin W. J. Am. Chem. Soc. 2008; 130:14358–14359. [PubMed: 18844356]
33. deKrafft KE, Xie Z, Cao G, Tran S, Ma L, Zhou OZ, Lin W. Angew. Chem. Int. Ed. 2009; 48:9901–9904.
34. Liu D, Huxford RC, Lin W. Angew. Chem. Int. Ed. 2011; 50:3696–3700.
35. Roming M, Lunsdorf H, Dittmar KEJ, Feldmann C. Angew. Chem. Int. Ed. 2010; 49:632–637.
36. Rieter WJ, Taylor KML, Lin W. J. Am. Chem. Soc. 2007; 129:9852–9853. [PubMed: 17645339]
37. Horcajada P, Chalati T, Serre C, Gillet B, Sebrie C, Baati T, Eubank JF, Heurtaux D, Clayette P, Kreuz C, Chang JS, Hwang YK, Marsaud V, Bories PN, Cynober L, Gil S, Ferey G, Couvreur P, Gref R. Nat. Mater. 2010; 9:172–178. [PubMed: 20010827]
38. Rieter WJ, Pott KM, Taylor KML, Lin W. J. Am. Chem. Soc. 2008; 130:11584–11585. [PubMed: 18686947]
39. Taylor-Pashow KML, Della Rocca J, Xie Z, Tran S, Lin W. J. Am. Chem. Soc. 2009; 131:14261–14263. [PubMed: 19807179]
40. Imaz I, Rubio-Martinez M, Garcia-Fernandez L, Garcia F, Ruiz-Molina D, Hernando J, Puntes V, Maspoch D. Chem. Commun. 2010; 46:4737–4739.
41. Miller SR, Heurtaux D, Baati T, Horcajada P, Greneche JM, Serre C. Chem. Commun. 2010; 46:4526–4528.
42. Krajinovic M, Moghrabi A. Pharmacogenomics. 2004; 5:819–834. [PubMed: 15469405]
43. Davis ME, Chen Z, Shin DM. Nat. Rev. Drug Discov. 2008; 7:771–782. [PubMed: 18758474]
44. Stathopoulos GP. Anti-Cancer Drugs. 2010; 21:732–736. [PubMed: 20671511]
45. Chen Y-H, Tsai C-Y, Huang P-Y, Chang M-Y, Cheng P-C, Chou C-H, Chen D-H, Wang C-R, Shiau A-L, Wu C-L. Mol. Pharmaceutics. 2007; 4:713–722.
46. Dhanikula RS, Argaw A, Bouchard J-F, Hildgen P. Mol. Pharm. 2008; 5:105–116. [PubMed: 18171013]
47. Kohler N, Sun C, Fichtenholtz A, Gunn J, Fang C, Zhang M. Small. 2006; 2:785–792. [PubMed: 17193123]
48. Kohler N, Sun C, Wang J, Zhang M. Langmuir. 2005; 21:8858–8864. [PubMed: 16142971]

49. Wosikowski K, Biedermann E, Rattel B, Breiter N, Jank P, Loser R, Jansen G, Peters GJ. Clin. Cancer Res. 2003; 9:1917–1926. [PubMed: 12738750]
50. Yang X, Zhang Q, Wang Y, Chen H, Zhang H, Gao F, Liu L. Colloid Surface B. 2008; 61:125–131.
51. Cavka JH, Jakobsen S, Olsbye U, Guillou C NL, Bordiga S, Lillerud KP. J. Am. Chem. Soc. 2008; 130:13850–13851. [PubMed: 18817383]
52. Ashley CE, Carnes EC, Phillips GK, Padilla D, Durfee PN, Brown PA, Hanna TN, Liu J, Phillips B, Carter MB, Carroll NJ, Jiang X, Dunphy DR, Willman CL, Petsev DN, Evans DG, Parikh AN, Chackerian W BW, Peabody DS, Brinker CJ. Nat. Mater. 2011; 10:389–397. [PubMed: 21499315]
53. Li J, Chen Y-C, Tseng Y-C, Mozumdar S, Huang L. J. Controlled Release. 2010; 142:416–421.
54. Liu J, Stace-Naughton A, Jiang X, Brinker CJ. J. Am. Chem. Soc. 2009; 131:1354–1355. [PubMed: 19173660]
55. Troutier A-L, Delair T, Pichot C, Ladavire C. Langmuir. 2005; 21:1305–1313. [PubMed: 15697275]
56. Chen H, MacDonald RC, Li S, Krett NL, Rosen ST, O'Halloran TV. J. Am. Chem. Soc. 2006; 128:13348–13349. [PubMed: 17031934]
57. Vilner BJ, John CS, Bowen WD. Cancer Res. 1995; 55:408–413. [PubMed: 7812973]
58. Aydar E, Palmer CP, Djamgoz MBA. Cancer Res. 2004; 64:5029–5035. [PubMed: 15289298]
59. Banerjee R, Tyagi P, Li S, Huang L. Int. J. Cancer. 2004; 112:693–700. [PubMed: 15382053]
60. John CS, Vilner BJ, Geyer BC, Moody T, Bowen WD. Cancer Res. 1999; 59:4578–4583. [PubMed: 10493511]
61. Ganapathy ME, Prasad PD, Huang W, Seth P, Leibach FH, Ganapathy V. J. Pharmacol. Exp. Ther. 1999; 289:251–260. [PubMed: 10087012]

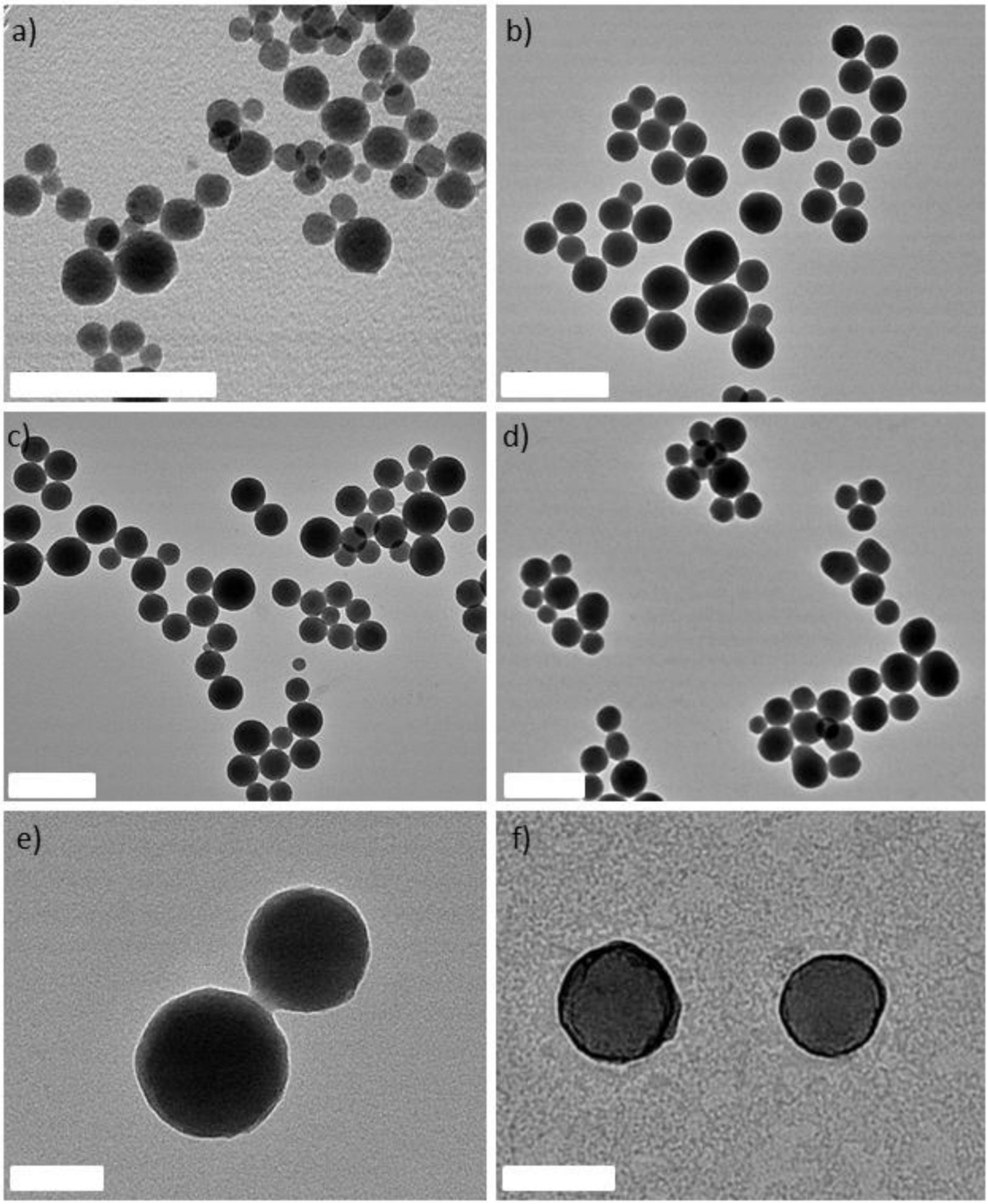

Figure 1.
TEM images of **1** (a), **2** (b), **3a** (c, e), and **3b** (d, f). The samples shown in e and f have been stained with uranyl acetate to highlight the lipid bilayer coating on **3b**. The scale bars represent 400 nm for a–d, and 100 nm for e–f.

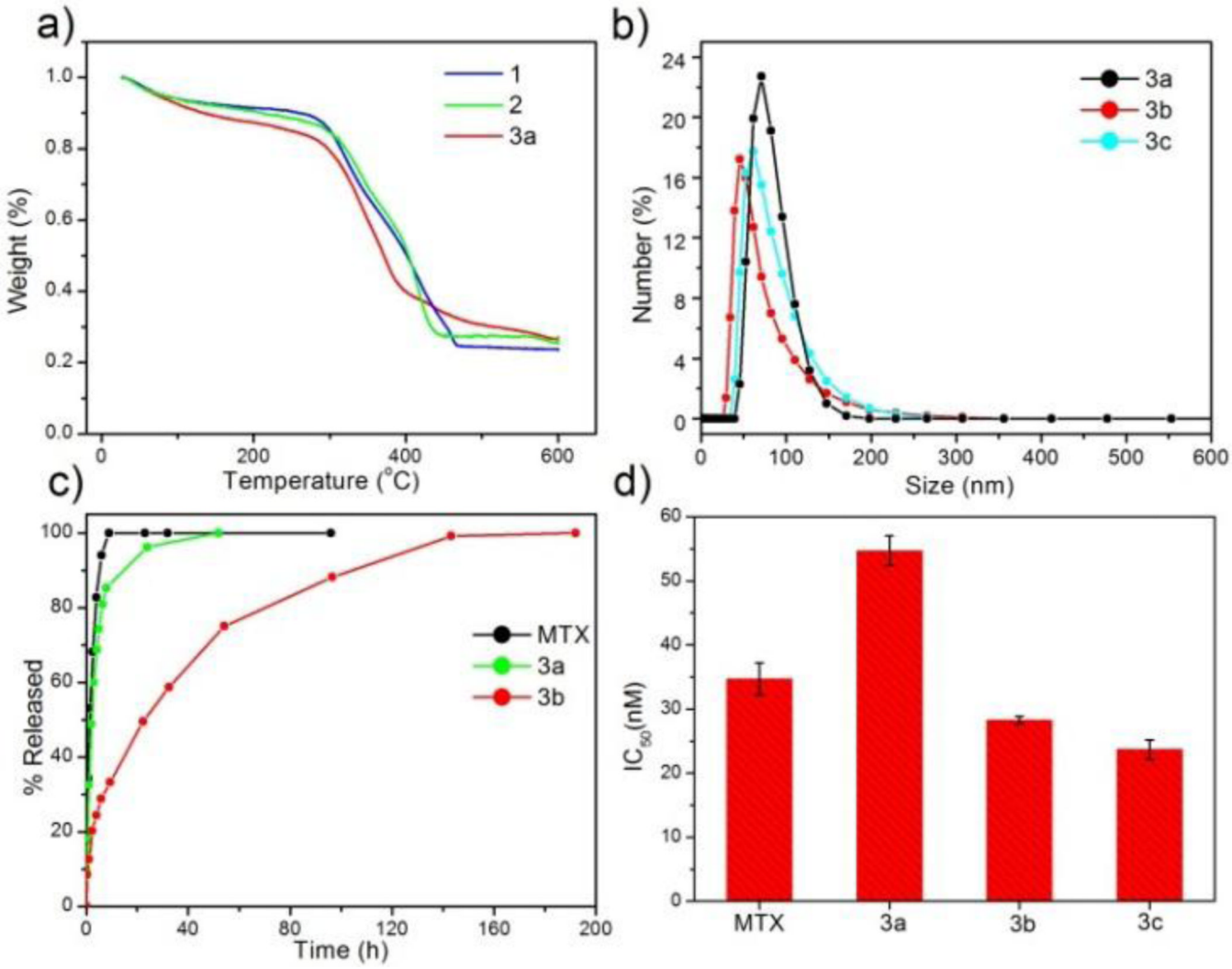

Figure 2.

a) TGA curves for **1, 2**, and **3a**. b) Particle size distributions for **3a, 3b**, and **3c** obtained by DLS. c) Release profiles in PBS for free MTX, **3a**, and **3b** obtained by measuring the release of MTX by UV-Vis spectroscopy. d) IC_{50} values for free MTX, **3a, 3b**, and **3c** obtained from *in vitro* cytotoxicity assays with a range of MTX concentrations against Jurkat human ALL cells. Error bars represent one standard deviation.

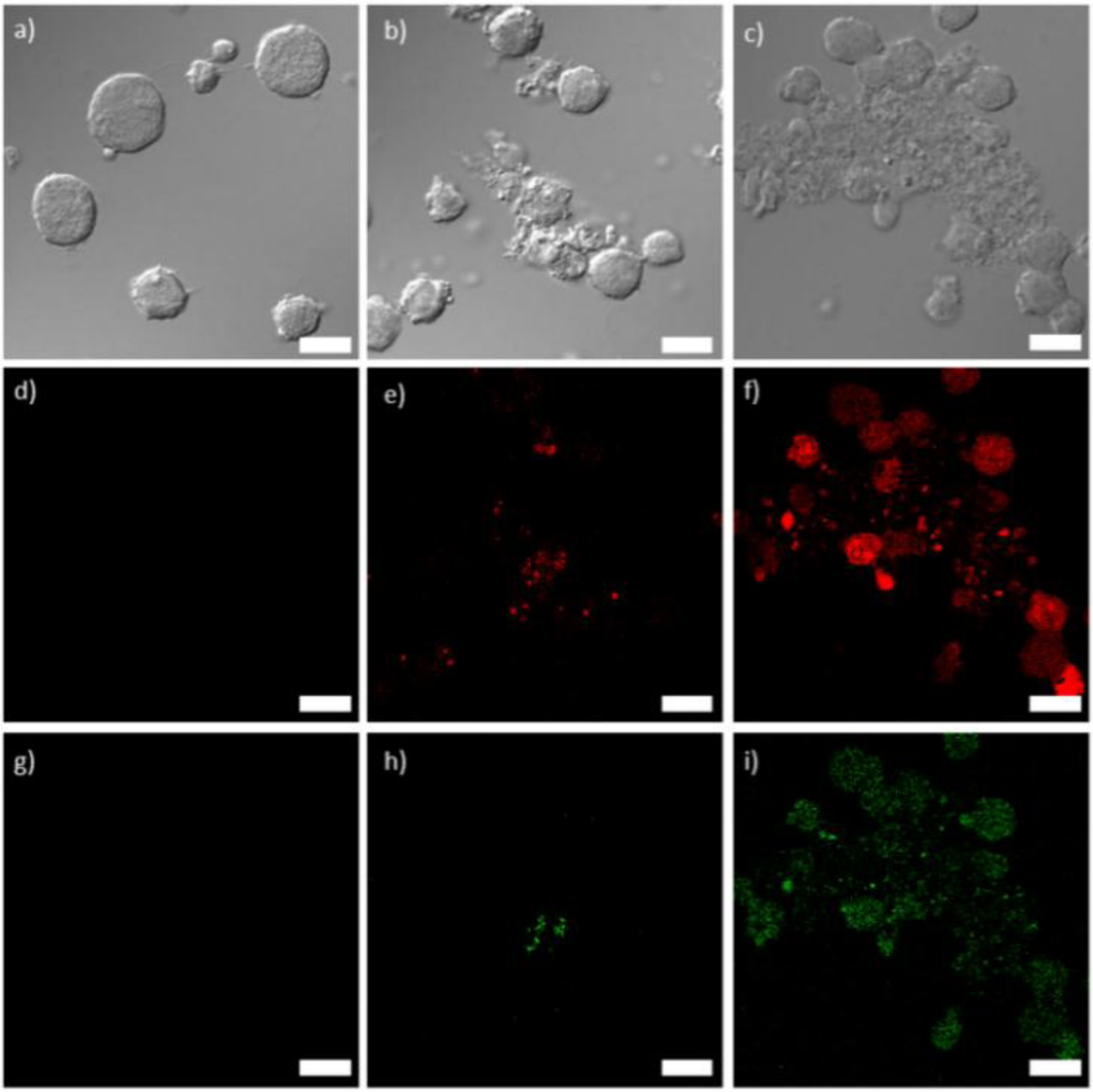

Figure 3.
a–c) Differential interference contrast (DIC) images and d–i) fluorescence images of Jurkat cells incubated with **3a** (d,g), **3b** (e,h), and **3c** (f,i). Red fluorescence (d–f) is from the $Ru(bpy)_3^{2+}$-doped particles and green fluorescence (g–i) is from the Annexin V FITC conjugate early apoptosis stain. Scale bars represent 25 μm.

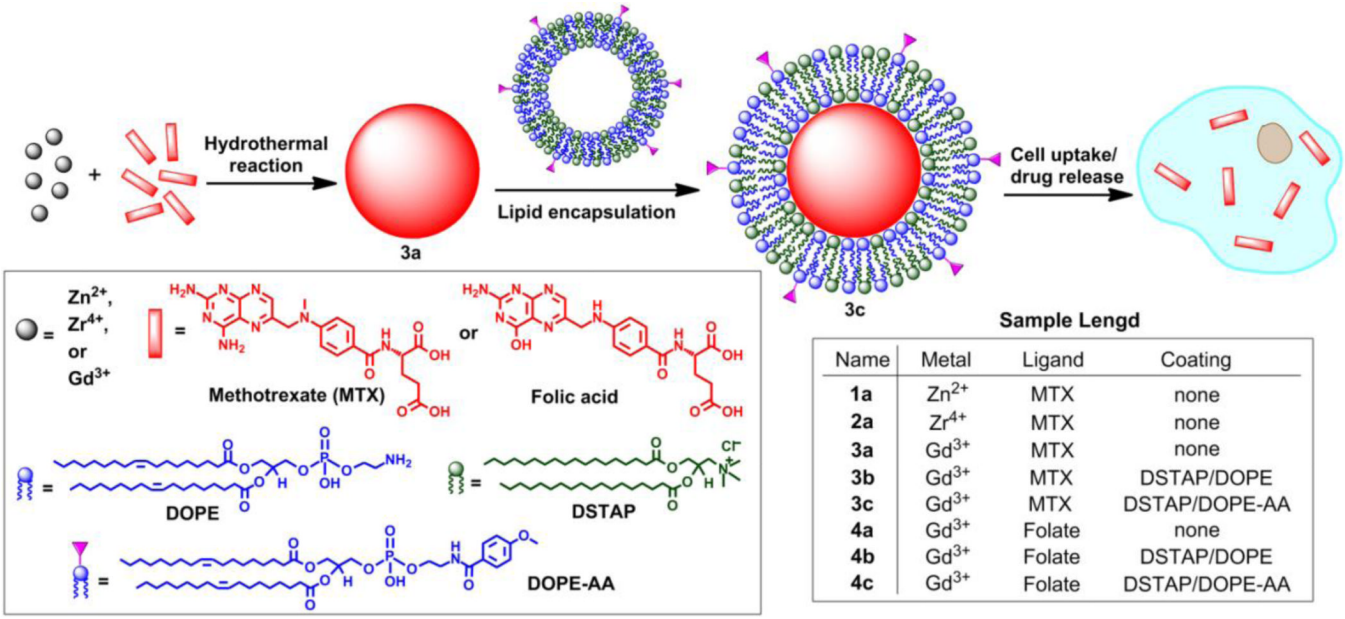

Sample Lengd

Name	Metal	Ligand	Coating
1a	Zn^{2+}	MTX	none
2a	Zr^{4+}	MTX	none
3a	Gd^{3+}	MTX	none
3b	Gd^{3+}	MTX	DSTAP/DOPE
3c	Gd^{3+}	MTX	DSTAP/DOPE-AA
4a	Gd^{3+}	Folate	none
4b	Gd^{3+}	Folate	DSTAP/DOPE
4c	Gd^{3+}	Folate	DSTAP/DOPE-AA

Scheme 1.
Synthesis of NCPs and functionalization of MTX-containing NCPs with a lipid bilayer and targeting moiety.

Table 1

DLS data[a] and MTX loadings[b] for MTX-based NCPs.

Sample	No. avg size (nm)	PDI	Zeta potential (mV)	wt % MTX
1	161[c]	0.20[c]	−1.9	79.1
2	88.4	0.18	−27.2	78.2
3a	77.7	0.04	−10.0	71.6
3b	64.6	0.24	32.6	~69.2[d]
3c	76.8	0.15	25.3	~69.0[d]

[a] Obtained in 1 mM aq. KCl unless otherwise noted.

[b] Determined from TGA data.

[c] Obtained in ethanol.

[d] Estimated based on lipid coating content.